

# Singlet-only Always-on Gapless Exchange Qubits with Baseband Control

Nathan L. Foulk,<sup>1</sup> Silas Hoffman,<sup>1,2</sup> Katharina Laubscher,<sup>1</sup> and Sankar Das Sarma<sup>1</sup>

<sup>1</sup>*Condensed Matter Theory Center and Joint Quantum Institute, Department of Physics, University of Maryland, College Park, Maryland 20742-4111 USA*

<sup>2</sup>*Laboratory for Physical Sciences, 8050 Greenmead Drive, College Park, Maryland 20740, USA*

We propose a singlet-only always-on gapless exchange (SAGE) spin qubit that encodes a single qubit in the spins of four electrons while allowing universal baseband control. While conventional exchange-only qubits suffer from magnetic-field-gradient-induced leakage and coherent errors, for instance due to local nuclear environments and variations in the  $g$ -factor, the SAGE qubit subspace is protected from coherent errors due to local magnetic field gradients and leakage out of the computational subspace is energetically suppressed due to the exchange interactions between electrons being always-on. Consequently, we find that when magnetic gradient noise dominates over charge noise, coherence times and single-qubit gate infidelities of the SAGE qubit improve by an order of magnitude compared to conventional exchange-only qubits. Moreover, using realistic parameters, two-qubit gates can be performed with a single interqubit exchange pulse with times comparable in duration to conventional exchange-only qubits but with a significantly simplified pulse sequence.

*Introduction.* Electrons localized in gate-defined semiconducting quantum dots are a promising candidate for building a large-scale fault-tolerant quantum computer. The most studied implementation is the so-called Loss-DiVincenzo (LD) qubit in which quantum information is encoded in the spin of a single electron [1–7]. Control of LD qubits typically necessitates ac electric fields (which causes heating effects) and on-chip micromagnets. These experimental requisites and the unreliable valley splitting in semiconducting two-dimensional electron gases have inhibited scale-up of LD qubits [8–12].

Alternatively, exchange-only (EO) qubits use three electrons localized to three quantum dots to form a single encoded qubit. EO qubits are so-named because there exist electrically controllable exchange interactions between the spins,  $H_{\text{exch}} = \sum_{i<j} J_{ij} \mathbf{s}_i \cdot \mathbf{s}_j$ , where  $J_{ij}$  is the magnitude of the exchange interaction between spin  $i$  and  $j$  and  $\mathbf{s}_j = (s_j^x, s_j^y, s_j^z)$  is a vector of the generators of rotation of the  $j$ th spin about  $x$ ,  $y$ , and  $z$  axis, respectively. These exchange interactions can be pulsed to access any point on the encoded qubit Bloch sphere. This all-electrical dc control and the absence of a micromagnet have drawn a large degree of experimental interest [13–20]. Although EO qubits are immune to global magnetic fields, coherence times and gate fidelities are limited by differences in local magnetic fields induced by, for instance, nuclear magnetic environments or differences in the  $g$ -factor between dots [21]. Specifically, these effective magnetic field gradients drive both coherent errors within the qubit subspace and cause leakage to noncomputational states.

There exists a singlet-only [22, 23] encoding of four electrons across four quantum dots which is immune to magnetic-field-gradient-induced coherent errors within the qubit subspace [24–29] while still retaining the control advantages of conventional EO qubits. Four electrons that are coupled through the exchange interaction with Hamiltonian  $H_{\text{exch}}$  can be used to define an encoded qubit whose states lie in the  $S = S^z = 0$  subspace, where

$S$  is the total spin quantum number and  $S^z$  is the quantum number associated with the eigenvalue of the spin operator along the  $z$ -axis. The qubit states in the singlet-only encoding are

$$|0\rangle = |S_{12}S_{34}\rangle, \quad (1)$$

$$|1\rangle = \frac{1}{\sqrt{3}} \left( |T_{12}^0 T_{34}^0\rangle - |T_{12}^+ T_{34}^-\rangle - |T_{12}^- T_{34}^+\rangle \right), \quad (2)$$

where  $|S_{ij}\rangle$  refers to a singlet spin state on dots  $i$  and  $j$  and  $|T_{ij}^0\rangle$ ,  $|T_{ij}^+\rangle$ , and  $|T_{ij}^-\rangle$  refer to triplet spin 0, 1, and  $-1$  states, respectively, on dots  $i$  and  $j$ . The four spins are coupled into pairs and the qubit state is determined from the spin parity of these pairs. Without a loss in generality, the spins of the first encoding pair are labeled as 1 and 2, and the other as 3 and 4.

Unfortunately, these singlet-only qubits are unprotected from leakage into noncomputational states driven by magnetic field gradients. Previous proposals for four-electron exchange qubits either did not address this problem [24–30], required an all-to-all connectivity that would be difficult to manufacture [31–35] or relied on ac driving of a gapped qubit [19, 22], which reintroduces the ac-induced heating that prompted the switch to exchange qubits.

*Qubit definition and coherence times.* We propose a singlet-only always-on gapless exchange-only (SAGE) spin qubit that provides protection from magnetic field gradients with scalable baseband control and suppressed leakage to noncomputational states. The SAGE qubit is implemented in a T-shape geometry as shown in Fig. 1(a), wherein there is an exchange interaction only between the electron in dot one and the electrons in dots two, three, and four. The resultant encoded qubit Hamiltonian is [see also the Supplemental Material (SM) [36]]

$$H_q = J_{14}(\sqrt{3}\sigma_x + \sigma_z) - J_{13}(\sqrt{3}\sigma_x - \sigma_z) - 2J_{12}\sigma_z. \quad (3)$$

The three axes of control [see Fig. 1(b)] allow the decreasing of the relevant exchange couplings to perform any ro

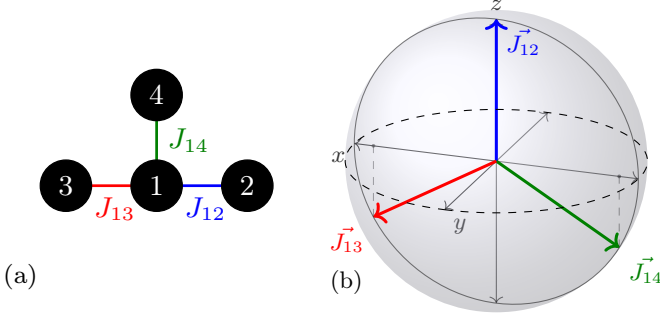


FIG. 1. *Qubit geometry and operation.* (a) A schematic of the SAGE qubit layout in real space. The encoding pairs of spins are  $\{1, 2\}$  and  $\{3, 4\}$ . (b) The Bloch sphere representation of the SAGE qubit and each exchange interaction's rotation axis of control.

tation in the  $x$ - $z$  plane—sufficient for accessing any state on the Bloch sphere. The T-geometry is further justified upon inspection of Eq. (3): when  $J_{12} = J_{13} = J_{14} = J$ , the computational states of the qubit are degenerate. This always-on, gapless operation improves on previous four-spin exchange qubits by energetically suppressing leakage while preserving dc control in the non-rotating frame. The spectral gap between the computational qubit states and noncomputational states—which suppresses leakage—is also maximized in this T-geometry, see SM [36].

SAGE qubit measurement is straightforward using Pauli spin blockade (PSB) [3, 22, 37, 38] so that electrons 1 and 2 are pulsed diabatically toward the same dot. A charge measurement then determines the qubit state [38] since the two electrons will only occupy the same dot if they form a singlet spin state, and we can thereby conclude that the encoded qubit is in the  $|0\rangle$  state. This charge measurement is reliable due to the singlet-triplet relaxation time being much longer than the charge relaxation time [39]. Similar to PSB measurements in conventional EO devices, the measurement is sufficient only when the qubit state is unleaked. SAGE qubit initialization can be performed by lowering the potential of two dots, and letting the spin states relax to two pairs of singlets after a long time before diabatically pulsing back so that the charge state is  $(N_1, N_2, N_3, N_4) = (1, 1, 1, 1)$ , where  $N_i$  is the electron number in the  $i$ th dot and the spin state is  $|0\rangle = |S_{12}\rangle |S_{34}\rangle$  [22].

The primary sources of decoherence in exchange-controlled qubits are magnetic field gradients and fluctuations in charge. The fluctuations in magnetic field gradients are modeled by a random magnetic field along the axis of quantization  $H_B = \sum_i h_i s_i^z$  [40] and fluctuations in charge are modeled by fluctuations in the exchange interaction between the localized electrons  $H_C = \sum_{i < j} J_{ij} \epsilon_{ij} \mathbf{s}_i \cdot \mathbf{s}_j$  with  $i, j = \{1, 2, 3, 4\}$ . These fluctuations are added to the underlying exchange Hamiltonian resulting in  $H = H_{\text{exch}} + H_B + H_C$ , where  $J_{ij}$  (con-

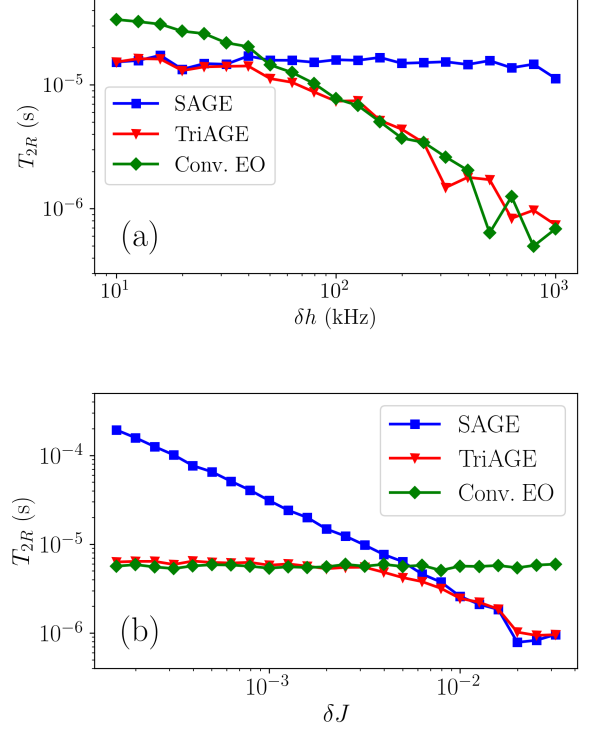


FIG. 2. *Qubit idle coherence times.* A survey of the average idle coherence time for several gapless exchange qubits. “TriAGE” refers to the triangular, always-on gapless exchange qubit, and “EO” refers to the conventional exchange-only qubit in a linear array. For the SAGE and TriAGE qubits, each exchange coupling is set to 10 MHz, whereas all of the conventional EO couplings are set to zero. These decays are averaged over 2500 realizations of magnetic and exchange disorder. (a) Coherence times of each system for a range of magnetic disorder strengths. Each time is extracted from a Gaussian fit of the average idle decay for each system with  $\delta J = 2 \times 10^{-3}$ . (b) Coherence times of each system for a range of relative exchange disorders with  $\delta h = 150$  kHz. Both  $\delta J = 2 \times 10^{-3}$  and  $\delta h = 150$  kHz reflect experimentally attainable parameters.  $H_C = 0$  for conventional EO systems, since  $J = 0$  for each coupling and the disorder is multiplicative.

tained in  $H_{\text{exch}}$  and  $H_C$ ) are only nonzero for spins  $i$  and  $j$  that are nearest neighbors as in Fig. 1(a). Upon initializing the encoded qubit along the  $x$  axis of the Bloch sphere, the state evolves according to a realization of the noise profile generated by sampling  $h_i$  ( $\epsilon_{ij}$ ) from a uniform distribution  $[-\delta h, \delta h]$  ( $[-\delta J, \delta J]$ ). The scale of magnetic disorder  $\delta h$  is assumed to be dependent on the underlying microscopics of the system and is therefore constant for a given realization. The quasistatic charge disorder  $\delta J$ , however, is well-documented to scale approximately linearly with the exchange coupling strength [41, 42]. Therefore, we vary the strength of disorder in our simulations by sweeping the values of

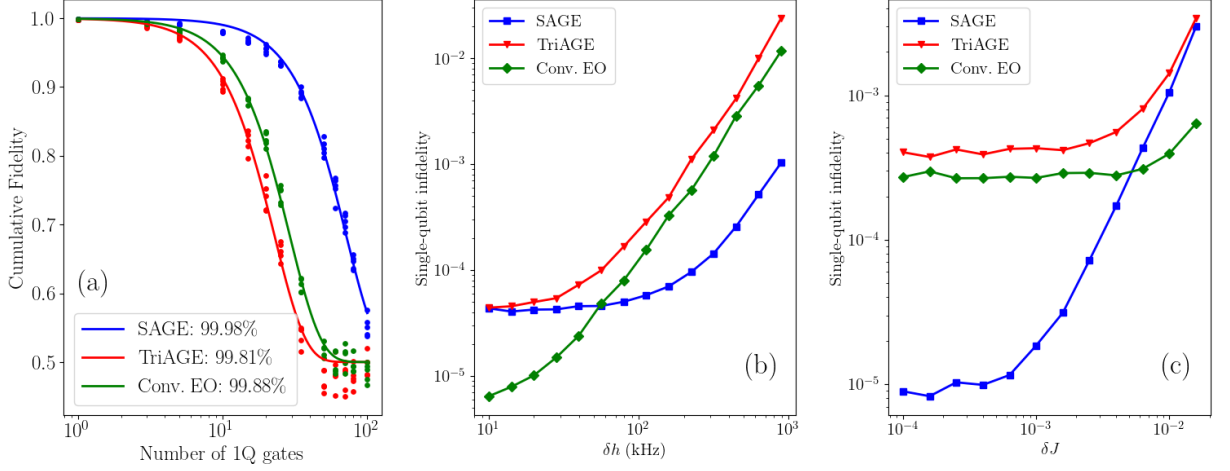


FIG. 3. *Single-qubit gate fidelities.* (a) Randomized benchmarking results for several gapless exchange qubits. Each point represents an average of 100 gate sequences of a given length, with each sequence averaged over 100 realizations of magnetic and exchange disorder with  $\delta h = 150$  kHz and  $\delta J = 2 \times 10^{-3}$ . (b) Fidelities extracted from randomized benchmarking over a sweep of values of  $\delta h$ , where  $\delta J = 2 \times 10^{-3}$ . The dashed lines correspond to zero charge noise  $\delta J = 0$ . (c) Fidelities extracted from randomized benchmarking over a sweep of values of  $\delta J$ , where  $\delta h$  is kept constant at 150 kHz.

unitful magnetic disorder  $\delta h$  and dimensionless charge disorder  $\delta J$ . The time-dependent off-diagonal element of the qubit density matrix is then averaged over 2500 realizations of noise and fit to  $A \exp[-(t/T_{2R})^2] + B$ , where  $T_{2R}$  is the Ramsey coherence time. To compare coherence times between exchange qubits, we also simulate and subsequently extract the coherence times for conventional EO qubits and the triangular always-on gapless exchange-only (TriAGE) analog to SAGE [13, 43], which is composed of three electrons in a triangular geometry.

We extract coherence times by first varying magnetic disorder while keeping charge disorder fixed at  $\delta J = 2 \times 10^{-3}$ , then varying charge disorder while keeping magnetic disorder constant at  $\delta h = 150$  kHz. For both the SAGE and TriAGE qubits, the interdot always-on exchange interaction is fixed at  $J_0 = 10$  MHz and for conventional EO qubits, the exchange is zero. For small magnetic disorder  $\delta h \lesssim 40$  kHz [Fig. 2(a)], the conventional EO qubit has a longer coherence time than both the SAGE and TriAGE qubits whose coherence times are roughly equal and constant. When the magnetic disorder is larger,  $\delta h \gtrsim 40$  kHz, the SAGE qubit has the longest coherence time and is roughly constant as a function of  $\delta h$  while the conventional EO and TriAGE qubits have roughly equal coherence times which decrease linearly with  $\delta h$ . This behavior is a consequence of the three-dot qubits being magnetic-disorder-dominated for large values of  $\delta h$ , whereas the SAGE qubit is limited by charge noise throughout Fig. 2(a).

Similarly, when fixing  $\delta h = 150$  kHz and varying  $\delta J$  as seen in Fig. 2(b), the SAGE qubit coherence time linearly decreases as  $\delta J$  is increased and has the best coherence times relative to the others when  $\delta J \lesssim 5 \times 10^{-3}$ . The

conventional EO is unaffected by fluctuations in charge noise since the exchange couplings vanish during a conventional EO idle, but the coherence time monotonically increases as the variance in magnetic gradient decreases. Because the SAGE qubit is most protected from magnetic noise when  $J_0 \gg \delta h$ —consistent with these parameters—the decoherence is dominated only by charge noise and is therefore roughly constant. Because the TriAGE qubit is susceptible to both coherent magnetic gradient variance and charge noise, it inherits poor coherence times over all values of  $\delta h$ .

*Single-qubit operation.* We characterize the fidelity of single-qubit gates using randomized benchmarking [44]. We apply  $N_{1Q}$  gates sampled from a set of single-qubit Cliffords (see SM [36]) for a given realization of disorder and average the fidelity over one hundred realizations of disorder and one hundred random gate sequences to obtain a cumulative fidelity [Fig. 3(a)]. For each single-qubit gate, we set the largest exchange coupling to a maximal exchange coupling  $J_0 = 10$  MHz. Because the error channel in this work is unitary, the exponential decay rate of the cumulative fidelity depends quadratically [45] on the sequence length  $N_{1Q}$  rather than the linear dependence often reported for devices exhibiting mostly depolarizing noise, having been manually fine-tuned to cancel out unitary errors [46].

We extract the single-qubit gate fidelity as a function of magnetic disorder  $\delta h$  while fixing  $\delta J$  [Fig. 3(b)]. When  $\delta h \lesssim 50$  kHz, the SAGE and TriAGE single-qubit gates are charge-noise-limited and have a worse fidelity than the conventional EO single-qubit gates, given  $\delta J = 2 \times 10^{-3}$ . For larger values of  $\delta h$ , the single-qubit gate infidelities are significantly improved for SAGE com-

pared to the TriAGE and conventional EO qubit fidelities. Fig. 3(c) illustrates the performance of single-qubit gates for various values of charge noise  $\delta J$ . Given a background magnetic disorder of  $\delta h = 150$  kHz, the maximum value of relative exchange disorder at which SAGE qubits outperform the two three-dot exchange qubits is approximately  $\delta J = 5 \times 10^{-3}$ .

The TriAGE qubit has, comparatively, the lowest single qubit fidelity for any value of disorder. The conventional EO qubit fidelity is nearly constant with respect to charge noise as seen in Fig. 3(c) up to  $\delta J \approx 4 \times 10^{-3}$ . This relationship differs qualitatively from that seen in the coherence times [Fig. 2(b)] and can be explained by single-qubit gates activating the multiplicative charge disorder prefactor in  $H_C$ . The value at which the SAGE single-qubit fidelity in Fig. 3(b) becomes magnetic-disorder-limited is approximately  $\delta h = 100$  kHz. Using the same parameters for idle coherence times in Fig. 2(a), this value was approximately  $\delta h = 1$  MHz. Thus we see that the SAGE qubit is especially resilient to magnetic disorder when idling, since the SAGE idle procedure features each exchange coupling tuned to its maximal value. Performing gates requires lowering the appropriate couplings, thereby weakening its energetic leakage suppression.

*Two-qubit operation.* Two-qubit gates can be performed on the SAGE qubit with a single interqubit exchange pulse of strength  $J_c$ . Although, in general, turning on an interqubit exchange interaction results in leakage to noncomputational states, this is suppressed by the always-on intraqubit exchange interactions. Therefore, to have good fidelity, we must operate in the regime where  $J_c \ll J_0$ . In this limit, we can perturbatively extract (see SM [36]) the effective interqubit interaction using a Schrieffer-Wolff transformation. A particularly simple effective two-qubit interaction

$$H_{2Q}^{\text{eff}} = (J_c^2/J_0)(-2\sigma_1^z - 2\sigma_2^z + 8\sigma_1^z\sigma_2^z)/3, \quad (4)$$

where  $\sigma_j^z$  is the Pauli matrix acting on the  $j$ th qubit, is achieved by pulsing the exchange interaction between each qubit's second electron (the electron that forms an encoding pair with the qubit's core electron—labeled 2 and 6 in Fig. 4(a)).

This interaction can be simulated exactly, i.e. using all computational and noncomputational states, using  $J_0 = 20$  MHz and  $J_c = 4$  MHz. We find that the gate resulting from this interaction is maximally entangling, and that the intrinsic fidelity of this gate (i.e. in the absence of disorder) is  $\sim 99.8\%$  with a two-qubit gate time of  $\sim 1.23 \mu\text{s}$ . This operation is equivalent to a CNOT up to single-qubit unitaries. The circuit diagram is shown in Fig. 4(b) and the operational details are presented in Table I. To demonstrate that this interaction is indeed maximally entangling, we simulate the effect of this two-qubit interaction on the entanglement entropy of an ini-

	$n_x$	$n_y$	$n_z$	$\phi$
$U_1$	0	0	1	$3\pi/4$
$U_2$	-0.3574	0.8629	-0.3574	1.71777
$U_3$	0	0	1	$-\pi/8$
$U_4$	-0.1915	-0.9626	-0.1915	1.60887

TABLE I. Single-qubit unitaries necessary to transform the  $J_c$  interaction to a CNOT gate. These unitaries  $U_i$  are labeled as shown in Fig. 4(b). Each single-qubit gate represents a rotation of angle  $\phi$  around the axis  $\hat{\mathbf{n}} = (n_x, n_y, n_z)$ .

tially separable state  $|\psi_0\rangle = \frac{1}{\sqrt{2}}(|00\rangle + |10\rangle)$  in Fig. 4(c) as a function of  $t$ , the duration of the  $J_c$  pulse.

Due to the limitation that  $J_c \ll J_0$ , the SAGE two-qubit gate is fidelity- and speed-limited by the ratio of intraqubit always-on interaction to interqubit exchange interaction. In particular, we numerically extract these general functional dependencies (see SM for details [36]) for the lower bound on the intrinsic fidelity for a two-qubit gate  $F_{\text{CNOT}}$  with a gate duration of  $t_{\text{CNOT}}$ :

$$F_{\text{CNOT}} \approx 1 - \frac{J_c^2}{2J_0^2}, \quad t_{\text{CNOT}} \approx \frac{J_0}{J_c^2}, \quad (5)$$

Gate fidelities can be improved beyond this lower bound through careful selection of  $J_c$  and  $J_0$  so that leakage fluctuations (as seen in Fig. 4(c)) are not the principal source of error. Increasing the maximal intraqubit exchange interaction enables faster and higher fidelity CNOT gates. For example, an intraqubit exchange interaction of  $J_0 = 100$  MHz would allow a commensurately larger  $J_c$  of 20 MHz, enabling a gate time  $\sim 123$  ns while maintaining  $\sim 99.8\%$  fidelity.

*Discussion and outlook.* The SAGE architecture's resilience to differences in Zeeman splitting makes it relatively immune to variations in the  $g$ -factor between dots. As a result, larger global magnetic fields could be applied to the SAGE qubits to polarize the nuclei. We expect that this will enhance the coherence times and gate fidelities of the SAGE qubit compared to the conventional EO qubit which suffers from poor qubit fidelities as the magnetic field is increased beyond  $\sim 1$  mT [15].

Although single-qubit operations can be performed by decreasing the intraqubit exchange interaction, one could alternatively increase the intraqubit exchange interaction. This novelty effectively enables clockwise and counterclockwise rotations about the three axes of the Bloch sphere described above. Consequently, simultaneous operation of two exchange interactions detuned in opposite directions from the always-on value, e.g.  $J_{14} = J_{12} + \Delta$  and  $J_{13} = J_{12} - \Delta$ , results in a rotation about the  $x$  axis. This allows any point on the Bloch sphere to be reached using two pulses.

As we have shown above, the speed at which one can perform two-qubit gates is largely limited by the intraqubit exchange interaction. Although we have taken

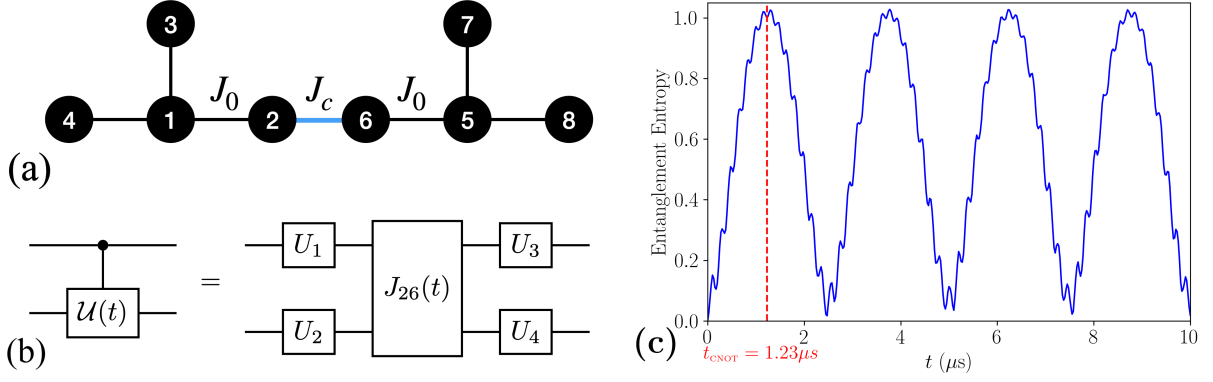


FIG. 4. *Two-qubit gates.* (a) An example geometry on which two-qubit gates can be performed using a single interqubit exchange pulse  $J_c = J_{26}$ . (b) A single  $J_{26}(t)$  pulse up to local unitaries is equivalent to a controlled- $\mathcal{U}(t)$  rotation.  $\mathcal{U}(t_{\text{CNOT}}) = X$  and the two-qubit circuit represents a CNOT gate. (c) A representative simulation of the von Neumann entanglement entropy of the initially separable state  $|\psi_0\rangle = \frac{1}{\sqrt{2}}(|00\rangle + |10\rangle)$  as a result of the SAGE two-qubit interaction with  $J_c = 4$  MHz and  $J_0 = 20$  MHz to facilitate a CNOT time  $t_{\text{CNOT}} = 1.23 \mu\text{s}$ .

modest values of exchange interaction throughout this article, exchange interactions  $\sim 10$  GHz have been demonstrated experimentally [15]. A full configuration interaction calculation would be useful to determine the maximal value that the always-on exchange interaction can take. Moreover, we expect that such a calculation would inform the most effective dot geometry for the above T-shaped connectivity.

Throughout the discussion of two-qubit gate fidelity, we have ignored disorder in the magnetic field gradients and charge disorder. Because noncomputational states are only explored virtually—in contrast to two-qubit gates in conventional EO qubits—we expect noise to affect two-qubit gates similarly to the way it affects single-qubit gates. Although beyond the scope of this article, a detailed calculation of these effects should be done in future studies.

We have shown that SAGE spin qubits can exhibit improved idle coherence times and higher single-qubit gate fidelities than similar exchange-only qubit designs. We have outlined a scheme for performing two-qubit gates, including the procedure for CNOT specifically using a single interqubit exchange pulse and local unitaries. We also verified its efficacy, showing that it is possible to perform a CNOT gate with  $\sim 99.8\%$  fidelity in a reasonable time.

The SAGE qubit offers a promising approach to the principal challenges facing the spin qubit community when it comes to scaling up, such as unavoidable magnetic field fluctuations, the heating effects of ac driving, and the impracticalities resulting from on-chip micro-magnets.

*Acknowledgments.* We thank N. Bishop, F. Mohiyaddin, and M. Curry for helpful discussions about experimental considerations and attainable parameter regimes. SH would like to thank A. Mills for valuable

discussions. This work was supported by the Laboratory for Physical Sciences.

- 
- [1] Daniel Loss and David P. DiVincenzo, “Quantum computation with quantum dots,” *Physical Review A* **57**, 120–126 (1998).
  - [2] Guido Burkard, Daniel Loss, and David P. DiVincenzo, “Coupled quantum dots as quantum gates,” *Physical Review B* **59**, 2070–2078 (1999).
  - [3] Guido Burkard, Thaddeus D. Ladd, Andrew Pan, John M. Nichol, and Jason R. Petta, “Semiconductor spin qubits,” *Reviews of Modern Physics* **95**, 025003 (2023).
  - [4] S Neyens, OK Zietz, TF Watson, F Luthi, A Nethewewala, HC George, E Henry, M Islam, AJ Wagner, F Borjans, EJ Connors, J Corrigan, MJ Curry, D Keith, R Kotlyar, LF Lampert, MT Mądzik, K Millard, FA Mohiyaddin, S Pellerano, R Pillarisetty, M Ramsey, R Savitskiy, S Schaal, G Zheng, J Ziegler, NC Bishop, S Bojarski, J Roberts, and JS Clarke, “Probing single electrons across 300-mm spin qubit wafers,” *Nature* **629**, 80–85 (2024).
  - [5] Hubert C. George, Mateusz T. Mądzik, Eric M. Henry, Andrew J. Wagner, Mohammad M. Islam, Felix Borjans, Elliot J. Connors, Joelle Corrigan, Matthew Curry, Michael K. Harper, Daniel Keith, Lester Lampert, Florian Luthi, Fahd A. Mohiyaddin, Sandra Murcia, Rohit Nair, Rambert Nahm, Aditi Nethewewala, Samuel Neyens, Roy D. Raharjo, Carly Rogan, Rostyslav Savitskiy, Thomas F. Watson, Josh Ziegler, Otto K. Zietz, Ravi Pillarisetty, Nathaniel C. Bishop, Stephanie A. Bojarski, Jeanette Roberts, and James S. Clarke, “12-spin-qubit arrays fabricated on a 300 mm semiconductor manufacturing line,” (2024), arXiv:2410.16583.
  - [6] Paul Steinacker, Nard Dumoulin Stuyck, Wee Han Lim, Tuomo Tantt, MengKe Feng, Andreas Nickl, Santiago Serrano, Marco Candido, Jesus D. Cifuentes, Fay E. Hudson, Kok Wai Chan, Stefan Kubicek, Julien Jussot,

- Yann Canvel, Sofie Beyne, Yosuke Shimura, Roger Loo, Clement Godfrin, Bart Raes, Sylvain Baudot, Danny Wan, Arne Laucht, Chih Hwan Yang, Andre Saraiva, Christopher C. Escott, Kristiaan De Greve, and Andrew S. Dzurak, “A 300 mm foundry silicon spin qubit unit cell exceeding 99% fidelity in all operations,” (2024), arXiv:2410.15590.
- [7] Asser Elsayed, Mohamed Shehata, Clement Godfrin, Stefan Kubicek, Shana Massar, Yann Canvel, Julien Jussot, George Simion, Massimo Mongillo, Danny Wan, Bogdan Govoreanu, Iuliana P. Radu, Ruoyu Li, Pol Van Dorpe, and Kristiaan De Greve, “Low charge noise quantum dots with industrial CMOS manufacturing,” (2022), arXiv:2212.06464.
- [8] Stephan G. J. Philips, Mateusz T. Mądzik, Sergey V. Amitonov, Sander L. de Snoo, Maximilian Russ, Nima Kalhor, Christian Volk, William I. L. Lawrie, Delphine Brousse, Larysa Tryputen, Brian Paquelet Wuetz, Amir Sammak, Menno Veldhorst, Giordano Scappucci, and Lieven M. K. Vandersypen, “Universal control of a six-qubit quantum processor in silicon,” *Nature* **609**, 919–924 (2022).
- [9] Xiao Xue, Maximilian Russ, Nodar Samkharadze, Brennan Undseth, Amir Sammak, Giordano Scappucci, and Lieven M. K. Vandersypen, “Computing with spin qubits at the surface code error threshold,” arXivNature 601, 343–347 (2022) , 2107.00628v1 (2021).
- [10] Akito Noiri, Kenta Takeda, Takashi Nakajima, Takashi Kobayashi, Amir Sammak, Giordano Scappucci, and Seigo Tarucha, “Fast universal quantum control above the fault-tolerance threshold in silicon,” (2021), arXiv:2108.02626.
- [11] Chien-An Wang, Valentin John, Hanifa Tidjani, Cécile X. Yu, Alexander S. Ivlev, Corentin Déprez, Floor van Riggelen-Doelman, Benjamin D. Woods, Nico W. Hendrickx, William I. L. Lawrie, Lucas E. A. Stehouwer, Stefan D. Oosterhout, Amir Sammak, Mark Friesen, Giordano Scappucci, Sander L. de Snoo, Maximilian Rimbach-Russ, Francesco Borsoi, and Menno Veldhorst, “Operating semiconductor quantum processors with hopping spins,” *Science* **385**, 447–452 (2024).
- [12] K. Takeda, J. Yoneda, T. Otsuka, T. Nakajima, M. R. Delbecq, G. Allison, Y. Hoshi, N. Usami, K. M. Itoh, S. Oda, T. Kadera, and S. Tarucha, “Optimized electrical control of a Si/SiGe spin qubit in the presence of an induced frequency shift,” (2018), arXiv:1810.12040.
- [13] Edwin Acuna, Joseph D. Broz, Kaushal Shyamsundar, Antonio B. Mei, Colin P. Feeney, Valerie Smetanka, Tiffany Davis, Kangmu Lee, Maxwell D. Choi, Brydon Boyd, June Suh, Wonill D. Ha, Cameron Jennings, Andrew S. Pan, Daniel S. Sanchez, Matthew D. Reed, and Jason R. Petta, “Coherent control of a triangular exchange-only spin qubit,” (2024), arXiv:2406.03705.
- [14] Irina Heinz, Felix Borjans, Matthew Curry, Roza Kotlyar, Florian Luthi, Mateusz T. Mądzik, Fahd A. Mohiyaddin, Nathaniel Bishop, and Guido Burkard, “Fast quantum gates for exchange-only qubits using simultaneous exchange pulses,” (2024), arXiv:2409.05843.
- [15] AJ Weinstein, MD Reed, AM Jones, RW Andrews, D Barnes, JZ Blumoff, LE Euliss, K Eng, BH Fong, SD Ha, DR Hulbert, CAC Jackson, M Jura, TE Keating, J Kerckhoff, AA Kiselev, J Matten, G Sabbir, A Smith, J Wright, MT Rakher, TD Ladd, and MG Borselli, “Universal logic with encoded spin qubits in silicon.” *Nature* **615**, 817–822 (2023).
- [16] Wonill Ha, Sieu D. Ha, Maxwell D. Choi, Yan Tang, Adele E. Schmitz, Mark P. Levendoff, Kangmu Lee, James M. Chappell, Tower S. Adams, Daniel R. Hulbert, Edwin Acuna, Ramsey S. Noah, Justine W. Matten, Michael P. Jura, Jeffrey A. Wright, Matthew T. Rakher, and Matthew G. Borselli, “A Flexible Design Platform for Si/SiGe Exchange-Only Qubits with Low Disorder,” *Nano Letters* **22**, 1443–1448 (2022).
- [17] Jacob Z. Blumoff, Andrew S. Pan, Tyler E. Keating, Reed W. Andrews, David W. Barnes, Teresa L. Brecht, Edward T. Croke, Larken E. Euliss, Jacob A. Fast, Clayton A.C. Jackson, Aaron M. Jones, Joseph Kerckhoff, Robert K. Lanza, Kate Raach, Bryan J. Thomas, Roland Velunta, Aaron J. Weinstein, Thaddeus D. Ladd, Kevin Eng, Matthew G. Borselli, Andrew T. Hunter, and Matthew T. Rakher, “Fast and High-Fidelity State Preparation and Measurement in Triple-Quantum-Dot Spin Qubits,” *PRX Quantum* **3**, 010352 (2022).
- [18] J. Kerckhoff, B. Sun, B.H. Fong, C. Jones, A.A. Kiselev, D.W. Barnes, R.S. Noah, E. Acuna, M. Akmal, S.D. Ha, J.A. Wright, B.J. Thomas, C.A.C. Jackson, L.F. Edge, K. Eng, R.S. Ross, and T.D. Ladd, “Magnetic Gradient Fluctuations from Quadrupolar  $^{73}\text{Ge}$  in Si / Si Ge Exchange-Only Qubits,” *PRX Quantum* **2**, 010347 (2021).
- [19] Maximilian Russ, J. R. Petta, and Guido Burkard, “Quadrupolar Exchange-Only Spin Qubit,” *Physical Review Letters* **121**, 177701 (2018).
- [20] Stefano Bosco and Maximilian Rimbach-Russ, “Exchange-Only Spin-Orbit Qubits in Silicon and Germanium,” (2024), arXiv:2410.05461.
- [21] The ability to fabricate samples with reliably large valley splittings practically has been achieved in recent years by uniformly doping the quantum well with germanium. These germanium nuclei are often spinful, making the problem of magnetic field disorder from nuclear spins an even more pressing challenge for all silicon spin qubits.
- [22] Arnau Sala and Jeroen Danon, “Exchange-only singlet-only spin qubit,” *Physical Review B* **95**, 241303(R) (2017).
- [23] Arnau Sala, Jørgen Holme Qvist, and Jeroen Danon, “Highly tunable exchange-only singlet-only qubit in a GaAs triple quantum dot,” *Physical Review Research* **2**, 012062(R) (2020).
- [24] Dave Bacon, Julia Kempe, Daniel A. Lidar, and K. B. Whaley, “Universal Fault-Tolerant Computation on Decoherence-Free Subspaces,” *Physical Review Letters* **85**, 1758–1761 (2000).
- [25] D. Bacon, D. A. Lidar, and K. B. Whaley, “Robustness of decoherence-free subspaces for quantum computation,” *Physical Review A* **60**, 1944–1955 (1999).
- [26] D. Bacon, J. Kempe, D. P. DiVincenzo, D. A. Lidar, and K. B. Whaley, “Encoded Universality in Physical Implementations of a Quantum Computer,” (2001), arXiv:quant-ph/0102140.
- [27] D. Bacon, *Decoherence, Control, and Symmetry in Quantum Computers*, PhD Thesis, arXiv (2003).
- [28] J. Kempe, D. Bacon, D. P. DiVincenzo, and K. B. Whaley, “Encoded Universality from a Single Physical Interaction,” (2001), arXiv:quant-ph/0112013.
- [29] J. Kempe, D. Bacon, D. A. Lidar, and K. B. Whaley, “Theory of decoherence-free fault-tolerant universal quantum computation,” *Physical Review A* **63**, 042307

- (2001).
- [30] M. Hsieh, J. Kempe, S. Myrgren, and K. B. Whaley, “An Explicit Universal Gate-set for Exchange-Only Quantum Computation,” (2003), arXiv: 0309002.
  - [31] Dave Bacon, Kenneth R. Brown, and K. B. Whaley, “Coherence-Preserving Quantum Bits,” *Physical Review Letters* **87**, 247902 (2001).
  - [32] Yaakov S. Weinstein, C. S. Hellberg, and Jeremy Levy, “Quantum-dot cluster-state computing with encoded qubits,” *Physical Review A* **72**, 020304(R) (2005).
  - [33] Yaakov S. Weinstein and C. S. Hellberg, “Scalable Architecture for Coherence-Preserving Qubits,” *Physical Review Letters* **98**, 110501 (2007).
  - [34] Bobby Antonio and Sougato Bose, “Two-qubit gates for decoherence-free qubits using a ring exchange interaction,” *Physical Review A* **88**, 042306 (2013).
  - [35] L. Jiang, A.M. Rey, O. Romero-Isart, J.J. Garcia-Ripoll, A. Sanpera, and M. D. Lukin, “Preparation of decoherence-free cluster states with optical superlattices,” *Physical Review A* **79**, 022309 (2009).
  - [36] See Supplemental Material.
  - [37] Leo Kouwenhoven and Charles Marcus, “Quantum dots,” *Physics World* **11**, 35 (1998).
  - [38] J. R. Petta, A. C. Johnson, J. M. Taylor, E. A. Laird, A. Yacoby, M. D. Lukin, C. M. Marcus, M. P. Hanson, and A. C. Gossard, “Coherent Manipulation of Coupled Electron Spins in Semiconductor Quantum Dots,” *Science* **309**, 2180–2184 (2005).
  - [39] Toshimasa Fujisawa, David Guy Austing, Yasuhiro Tokura, Yoshiro Hirayama, and Seigo Tarucha, “Allowed and forbidden transitions in artificial hydrogen and helium atoms,” *Nature* **419**, 278–281 (2002), arXiv:cond-mat/0209464.
  - [40] The assumption that magnetic disorder is polarized along the axis of quantization is justified by the SAGE qubit’s resilience to  $g$ -factor variation. A large global magnetic field can then be applied to the system—polarizing the background nuclear spins.
  - [41] M. D. Reed, B. M. Maune, R. W. Andrews, M. G. Borselli, K. Eng, M. P. Jura, A. A. Kiselev, T. D. Ladd, S. T. Merkel, I. Milosavljevic, E. J. Pritchett, M. T. Rakher, R. S. Ross, A. E. Schmitz, A. Smith, J. A. Wright, M. F. Gyure, and A. T. Hunter, “Reduced sensitivity to charge noise in semiconductor spin qubits via symmetric operation,” *Physical Review Letters* **116**, 110402 (2016).
  - [42] M. D. Shulman, O. E. Dial, S. P. Harvey, H. Bluhm, V. Umansky, and A. Yacoby, “Demonstration of Entanglement of Electrostatically Coupled Singlet-Triplet Qubits,” *Science* **336**, 202–205 (2012).
  - [43] Yaakov S. Weinstein and C. S. Hellberg, “Energetic suppression of decoherence in exchange-only quantum computation,” *Physical Review A* **72**, 022319 (2005).
  - [44] E. Knill, D. Leibfried, R. Reichle, J. Britton, R. B. Blakestad, J. D. Jost, C. Langer, R. Ozeri, S. Seidelin, and D. J. Wineland, “Randomized benchmarking of quantum gates,” *Physical Review A* **77**, 012307 (2008).
  - [45] Sarah Sheldon, Lev S. Bishop, Easwar Magesan, Stefan Filipp, Jerry M. Chow, and Jay M. Gambetta, “Characterizing errors on qubit operations via iterative randomized benchmarking,” *Physical Review A* **93**, 012301 (2016).
  - [46] The minimization of quadratically-scaling correlated errors is nonetheless extremely relevant, since such hand-tuning of microscopic level disorder is likely not feasible for large-scale devices. Nevertheless, the correlated error fidelity presented here and uncorrelated error fidelity seen in linear scaling are different quantities.
  - [47] Yuriy Makhlin, “Nonlocal Properties of Two-Qubit Gates and Mixed States, and the Optimization of Quantum Computations,” *Quantum Information Processing* **1**, 243–252 (2002).



## Supplemental Material: Singlet-only Always-on Gapless Exchange Qubits with Baseband Control

### SINGLE-QUBIT HAMILTONIANS

#### Four-electron Hamiltonian

The disordered Heisenberg Hamiltonian with an onsite Zeeman term,

$$H = \sum_{\langle i,j \rangle} J_{ij} \mathbf{s}_i \cdot \mathbf{s}_j + \sum_i h_i s_i^z, \quad (S1)$$

restricts single-qubit dynamics to a certain  $S_z$  subspace. For the SAGE qubit, we work in the  $S_z = 0$  subspace of a four-electron system. This subspace is spanned by six states  $|0\rangle$ ,  $|1\rangle$ ,  $|T_1\rangle$ ,  $|T_2\rangle$ ,  $|T_3\rangle$ , and  $|Q\rangle$  that can be characterized by the quantum numbers  $S$ ,  $S_{12}$ , and  $S_{34}$ , where  $S_{12}$  ( $S_{34}$ ) is the total spin angular momentum eigenvalue for the electron pair  $\{1,2\}$  ( $\{3,4\}$ ):

	$ 0\rangle$	$ 1\rangle$	$ T_1\rangle$	$ T_2\rangle$	$ T_3\rangle$	$ Q\rangle$
$S$	0	0	1	1	1	2
$S_{12}$	0	1	0	1	1	1
$S_{34}$	0	1	1	0	1	1
$S_z$	0	0	0	0	0	0

In this basis,  $H$  (restricted to the  $S_z = 0$  subspace) has the matrix representation

$$H_{1Q}^{4\text{-dot}} = \begin{pmatrix} -3J_a & \sqrt{3}(J_c - J_b) & -\Delta_{34} & -\Delta_{12} & 0 & 0 \\ \sqrt{3}(J_c - J_b) & J_a - 2(J_b + J_c) & \frac{1}{\sqrt{3}}\Delta_{12} & \frac{1}{\sqrt{3}}\Delta_{34} & \sqrt{\frac{2}{3}}(-\Delta_{13} - \Delta_{24}) & 0 \\ -\Delta_{34} & \frac{1}{\sqrt{3}}\Delta_{12} & -J_a - 2J_{\Delta a} & J_b - J_c & -\sqrt{2}(J_{\Delta b} + J_{\Delta c}) & -\sqrt{\frac{2}{3}}\Delta_{12} \\ -\Delta_{12} & \frac{1}{\sqrt{3}}\Delta_{34} & J_b - J_c & 2J_{\Delta a} - J_a & \sqrt{2}(J_{\Delta b} - J_{\Delta c}) & -\sqrt{\frac{2}{3}}\Delta_{34} \\ 0 & \sqrt{\frac{2}{3}}(-\Delta_{13} - \Delta_{24}) & -\sqrt{2}(J_{\Delta b} + J_{\Delta c}) & \sqrt{2}(J_{\Delta b} - J_{\Delta c}) & J_a - J_b - J_c & \frac{-\Delta_{13} - \Delta_{24}}{\sqrt{3}} \\ 0 & 0 & -\sqrt{\frac{2}{3}}\Delta_{12} & -\sqrt{\frac{2}{3}}\Delta_{34} & \frac{-\Delta_{13} - \Delta_{24}}{\sqrt{3}} & J_a + J_b + J_c \end{pmatrix},$$

where  $\Delta_{ij} = h_i - h_j$ ,  $J_a = J_{12} + J_{34}$ ,  $J_b = J_{13} + J_{24}$ ,  $J_c = J_{14} + J_{23}$ ,  $J_{\Delta a} = J_{12} - J_{34}$ ,  $J_{\Delta b} = J_{13} - J_{24}$ , and  $J_{\Delta c} = J_{14} - J_{23}$ . When setting  $J_{23} = J_{24} = J_{34} = 0$  in the absence of magnetic disorder, we obtain the single-qubit Hamiltonian given in Eq. (3) of the main text up to a constant shift.

$H_{1Q}^{4\text{-dot}}$  makes it visually clear that magnetic field gradients only couple states that have different values of  $S$ . To ensure optimal energetic suppression of leakage, the energy gaps between the computational states with  $S = 0$  and the leakage states with  $S = 1, 2$  should be maximized. At the same time, the computational states should remain degenerate to allow for gapless operation of the qubit.

Diagonalizing  $H_{1Q}^{4\text{-dot}}$  in the absence of magnetic disorder, we find that gapless operation requires  $J_a = J_b = J_c = J$ , so that both qubit states have energy  $-3J$ . Furthermore, the gaps between computational and leakage states are found to reach a maximal value of  $2J$  at two optimal points in parameter space. The first optimal point is  $J_{\Delta a} = J_{\Delta b} = J_{\Delta c} = \pm J$ , which implies a T-shape geometry, as outlined in the main text. The second optimal point is  $J_{\Delta a} = J_{\Delta b} = J_{\Delta c} = 0$ , which implies a box-shape geometry with all-to-all connectivity. This second geometry has been explored theoretically [S31–S35] but would be significantly more difficult to implement in quantum dots than the simple T-shape we propose. Other simple geometries such as a linear array or a square loop are incompatible with the  $J_a = J_b = J_c$  requirement, and therefore cannot be used for SAGE qubits.

#### Three-electron Hamiltonian

For the three-electron encodings discussed in the main text, i.e., the conventional EO qubit and the always-on gapless exchange qubit (TriAGE), we work in the total  $S_z = 1/2$  subspace of a three-electron system. This subspace



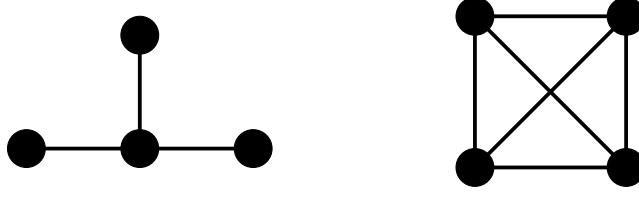


FIG. S1. The two optimal gapless qubit geometries to ensure maximal leakage suppression. Other geometries are possible for four-electron always-on qubits, but they are either not gapless—such as a linear array—or suffer from enhanced leakage compared to these two geometries.

is spanned by three states  $|S, S_{12}\rangle = \{|\frac{1}{2}, 0\rangle, |\frac{1}{2}, 1\rangle, |\frac{3}{2}, 1\rangle\}$ . The first two states are the computational states, while the third state is a leakage state. The computational states are given by

$$|0\rangle = |\frac{1}{2}, 0\rangle = |S\rangle|\uparrow\rangle,$$

$$|1\rangle = |\frac{1}{2}, 1\rangle = \frac{1}{\sqrt{3}}\left(\sqrt{2}|T_+\rangle|\downarrow\rangle - |T_0\rangle|\uparrow\rangle\right),$$

where  $|S\rangle = (|\uparrow\downarrow\rangle - |\downarrow\uparrow\rangle)/\sqrt{2}$ ,  $|T_0\rangle = (|\uparrow\downarrow\rangle + |\downarrow\uparrow\rangle)/\sqrt{2}$ , and  $|T_+\rangle = |\uparrow\uparrow\rangle$ . The Hamiltonian defined in Eq. (S1), restricted to the total  $S_z = 1/2$  subspace, can then be expressed in matrix form (up to a constant energy offset) as:

$$H_{1Q}^{3\text{-dot}} = \frac{1}{3} \begin{pmatrix} \Delta_{12} + \Delta_{23} - 9J_{12} & \sqrt{3}(\Delta_{12} - 3J_{13} + 3J_{23}) & -\sqrt{6}\Delta_{12} \\ \sqrt{3}(\Delta_{12} - 3J_{13} + 3J_{23}) & -\Delta_{12} - \Delta_{23} + 3J_{12} - 6(J_{13} + J_{23}) & -\sqrt{2}(\Delta_{13} + \Delta_{23}) \\ -\sqrt{6}\Delta_{12} & -\sqrt{2}(\Delta_{13} + \Delta_{23}) & 3(J_{12} + J_{13} + J_{23}) \end{pmatrix},$$

where  $\Delta_{ij} = h_i - h_j$ . Unlike the four-dot case,  $H_{1Q}^{3\text{-dot}}$  couples computational states, making the energetic suppression of magnetic-gradient-induced errors impossible.

### SINGLE-QUBIT GATES USED IN RANDOMIZED BENCHMARKING

Our randomized benchmarking results in the main text are calculated after initializing the qubit to the state  $|\psi\rangle = \frac{1}{\sqrt{2}}(|0\rangle + i|1\rangle)$  using single-qubit gates whose rotation axes lie in the  $x$ - $z$  plane of the Bloch sphere of the encoded qubit. This allows each gate to be performed in a single time step. The exchange strengths and gate durations are given in Table I.

SAGE					TriAGE				Conv. EO		
	$J_{12}$	$J_{13}$	$J_{14}$	$t$		$J_{12}$	$J_{23}$	$J_{13}$	$t$		$J_{12}$ $J_{13}$ $t$
$I$	10	10	10	$\pi/10$	$I$	10	10	10	$\pi/10$	$I$	0 0 $\pi/20$
$X$	20/3	10	10/3	$\sqrt{3}\pi/20$	$X$	20/3	10	10/3	$\sqrt{3}\pi/20$	$X$	0 10 $\pi/20$
$Z$	10	10	5	$\pi/10$	$Z$	10	10	5	$\pi/10$	$Z$	10 0 $\pi/20$
$H$	$5 \cdot (1 - \frac{1}{\sqrt{3}})$	10	$10 \cdot (1 - \frac{1}{\sqrt{3}})$	$\sqrt{2}\pi/20$	$H$	$5 \cdot (1 - \frac{1}{\sqrt{3}})$	10	$10 \cdot (1 - \frac{1}{\sqrt{3}})$	$\sqrt{2}\pi/20$		

TABLE I. The exchange interaction strengths of each single-qubit gate in randomized benchmarking in the main text. Each exchange strength is expressed in units of MHz and the gate durations in units of  $\mu s$ .  $I$ ,  $X$ ,  $Z$ , and  $H$  represent the standard quantum computing operations of identity, X, Z, and Hadamard.  $N$  represents a  $\pi$ -pulse about the  $\hat{n} = \frac{1}{2}(\sqrt{3}\hat{x} - \hat{z})$  direction and was included due to its status as a single-pulse qubit operation similar to the other gates included in the randomized benchmarking procedure. Performing a  $X$  or  $H$  gate would require more than one pulse using conventional EO qubits.

### CHARACTERIZATION OF THE SAGE TWO-QUBIT GATE

We perform a Schrieffer-Wolff transformation to understand the effective two-qubit Hamiltonian for the geometry shown in Fig. 4(a) of the main text—where  $J_{26} = J_c$  is the only nonzero interqubit coupling, and all intraqubit couplings are set to  $J_0 = 20$  MHz—and obtain up to third order in  $J_c/J_0$ :

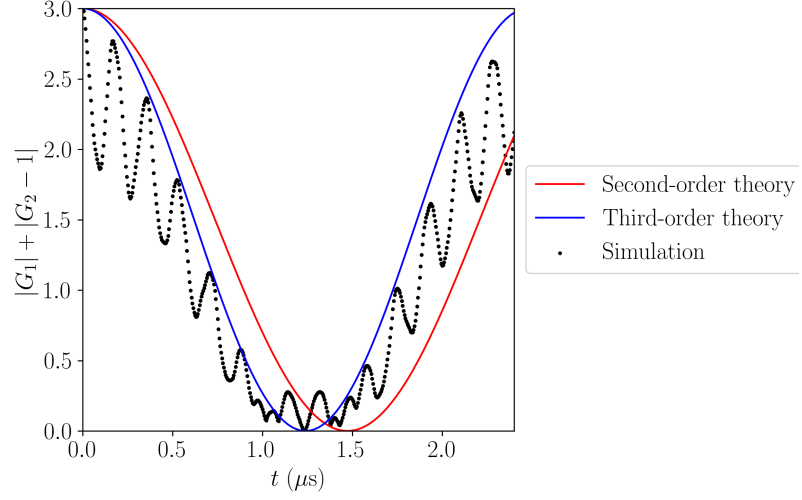


FIG. S2. Norm of the deviation of the Makhlin invariants ( $G_1, G_2$ ) from the correct CNOT invariants. At each time step, the unitary is computed where  $J_{26} = 0.2J_0 = 4$  MHz is the only nonzero interqubit coupling. The Makhlin invariants corresponding to CNOT are  $G_1 = 0$  and  $G_2 = 1$ .

$$H_{\text{eff}} = \frac{J_c^2}{32J_0} \begin{pmatrix} -12 - 3J_c/J_0 & 0 & 0 & 0 \\ 0 & -44 - 39J_c/J_0 & 0 & 0 \\ 0 & 0 & -44 - 39J_c/J_0 & 0 \\ 0 & 0 & 0 & \frac{28}{3} + 5J_c/J_0 \end{pmatrix}, \quad (\text{S2})$$

where our basis is  $|00\rangle, |01\rangle, |10\rangle, |11\rangle$ . The leading terms in Eq. S2 are equivalent to Eq. 4 in the main text. The first order terms We then compare this analytical result with the exact numerical simulation of the two-qubit gate in Fig. S2, where we compute the Makhlin invariants [S47] of the gate at each time step to find a gate equivalent to CNOT up to local unitaries. We find that a second-order Schrieffer-Wolff transformation captures the general evolution to CNOT and a third-order transformation correctly reproduces the CNOT gate time as predicted by numerics, although leakage oscillations which significantly impact the fidelity are visible in the numerical results.

The Makhlin invariants of a two-qubit unitary  $U$  are computed by converting  $U$  into the Bell basis via the transformation  $M_B = Q^\dagger U Q$ , where

$$Q = \frac{1}{\sqrt{2}} \begin{pmatrix} 1 & 0 & 0 & i \\ 0 & i & 1 & 0 \\ 0 & i & -1 & 0 \\ 1 & 0 & 0 & -i \end{pmatrix}. \quad (\text{S3})$$

The invariants are given as  $G_1 = \text{tr}(m)^2 \det U^\dagger / 16$  and  $G_2 = (\text{tr}(m)^2 - \text{tr}(m^2)) \det U^\dagger / 4$ , where  $m = M_B^T M_B$ . For the CNOT gate, we find that the Makhlin invariants are  $G_1 = 0$  and  $G_2 = 1$ .

We simulate CNOT gates over several values of  $J_0$  and  $J_c$  and find that a lower bound estimate of the intrinsic fidelity is given by the relationship  $F \approx 1 - \frac{J_c^2}{2J_0^2}$ . The time of the gate can be estimated as  $t_{\text{CNOT}} \approx J_0/J_c^2$ , plus the time of the significantly faster single-qubit unitaries. The numerical results illustrating these trends are shown in Fig. S3.

#### FOUR-ELECTRON INTERQUBIT COUPLINGS

In all, there are sixteen possible interqubit exchange couplings. Because the matrix elements of the interqubit exchange interactions between computational states are zero, all effective two-qubit interactions are of order  $J_c^2/J_0$ . We perform a Schrieffer-Wolff transformation from turning on a single interqubit exchange coupling and calculate each effective Hamiltonian to be

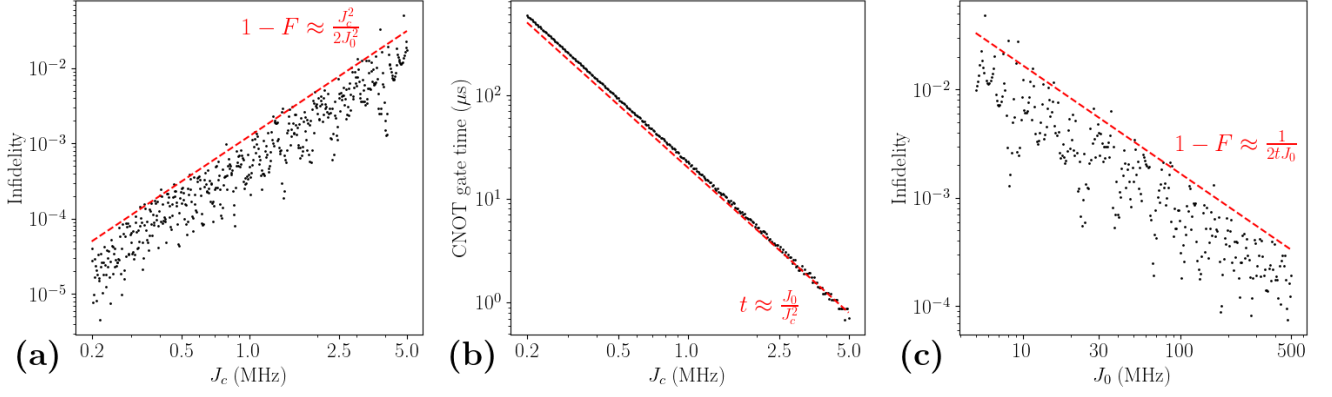


FIG. S3. Characterization of the two-qubit gate time and intrinsic fidelity for various values of  $J_0$  and  $J_c$ . (a) The intrinsic fidelity of the CNOT gate for a set value of  $J_0 = 20$  MHz. The exact value of  $F$  is generally unpredictable due to fluctuations from leakage. The red line represents a lower bound on the intrinsic fidelity. (b) The numerically found optimal gate times for the same value of  $J_0 = 20$  MHz. (c) Holding the gate time constant at  $t = 3 \mu\text{s}$ , the fidelity over a range of values of  $J_0$ .  $J_c = \sqrt{J_0/3} \mu\text{s}$  in order to fix the estimated gate time.

Exchange coupling $J_c$	Effective Hamiltonian (units of $J_c^2/J_0$ )
$J_{15}$	Identity
$J_{16}$	$2\sigma_1^z$
$J_{17}$	$\sqrt{3}\sigma_1^x - \sigma_1^z$
$J_{18}$	$-\sqrt{3}\sigma_1^x - \sigma_1^z$
$J_{25}$	$2\sigma_2^z$
$J_{26}$	$(-2\sigma_1^z - 2\sigma_2^z + 8\sigma_1^z\sigma_2^z)/3$
$J_{27}$	$(\sigma_1^z - 2\sigma_2^z - \sqrt{3}\sigma_1^x + 4\sqrt{3}\sigma_1^x\sigma_2^z - 4\sigma_1^z\sigma_2^z)/3$
$J_{28}$	$(\sigma_1^z - 2\sigma_2^z + \sqrt{3}\sigma_1^x - 4\sqrt{3}\sigma_1^x\sigma_2^z - 4\sigma_1^z\sigma_2^z)/3$
$J_{35}$	$\sqrt{3}\sigma_2^x - \sigma_2^z$
$J_{36}$	$(\sigma_2^z - 2\sigma_1^z - \sqrt{3}\sigma_2^x + 4\sqrt{3}\sigma_1^z\sigma_2^x - 4\sigma_1^z\sigma_2^z)/3$
$J_{37}$	$(\sigma_1^z + \sigma_2^z - \sqrt{3}\sigma_1^x - \sqrt{3}\sigma_2^x - 2\sqrt{3}\sigma_1^z\sigma_2^x - 2\sqrt{3}\sigma_1^x\sigma_2^z + 6\sigma_1^x\sigma_2^x + 2\sigma_1^z\sigma_2^z)/3$
$J_{38}$	$(\sigma_1^z + \sigma_2^z + \sqrt{3}\sigma_1^x - \sqrt{3}\sigma_2^x - 2\sqrt{3}\sigma_1^z\sigma_2^x + 2\sqrt{3}\sigma_1^x\sigma_2^z - 6\sigma_1^x\sigma_2^x + 2\sigma_1^z\sigma_2^z)/3$
$J_{45}$	$-\sqrt{3}\sigma_2^x - \sigma_2^z$
$J_{46}$	$(\sigma_2^z - 2\sigma_1^z + \sqrt{3}\sigma_2^x - 4\sqrt{3}\sigma_1^z\sigma_2^x - 4\sigma_1^z\sigma_2^z)/3$
$J_{47}$	$(\sigma_1^z + \sigma_2^z - \sqrt{3}\sigma_1^x + \sqrt{3}\sigma_2^x + 2\sqrt{3}\sigma_1^z\sigma_2^x - 2\sqrt{3}\sigma_1^x\sigma_2^z - 6\sigma_1^x\sigma_2^x + 2\sigma_1^z\sigma_2^z)/3$
$J_{48}$	$(\sigma_1^z + \sigma_2^z + \sqrt{3}\sigma_1^x + \sqrt{3}\sigma_2^x + 2\sqrt{3}\sigma_1^z\sigma_2^x + 2\sqrt{3}\sigma_1^x\sigma_2^z + 6\sigma_1^x\sigma_2^x + 2\sigma_1^z\sigma_2^z)/3$

The two-qubit basis used for these expressions is  $\{|00\rangle, |01\rangle, |10\rangle, |11\rangle\}$  where  $S_{12} = S_{34} = 0$  for state  $|0\rangle$  and  $S_{12} = S_{34} = 1$  for state  $|1\rangle$ .